OPEN ACCESS
IOP Publishing | International Atomic Energy Agency
Nuclear Fusion
Nucl. Fusion **66** (2026) 036050 (10pp)
https://doi.org/10.1088/1741-4326/ae463f

Verification of global gyrokinetic simulation of low frequency mode excited by thermal plasma in spherical tokamak

Handi Huang[1], Nikolai Gorelenkov[2], Xishuo Wei[1], Zhihong Lin[1,*], V.N. Duarte[2], Stanley Kaye[2] and Michele Romanelli[3]

[1] Department of Physics and Astronomy, University of California, Irvine, CA 92697, United States of America
[2] Princeton Plasma Physics Laboratory, Princeton, NJ 08540, United States of America
[3] Tokamak Energy Ltd, 173 Brook Drive, Milton Park, Oxfordshire OX14 4SD, United Kingdom of Great Britain and Northern Ireland

E-mail: zhihongl@uci.edu

Received 30 September 2025, revised 31 January 2026
Accepted for publication 16 February 2026
Published 26 February 2026

Abstract

A low frequency Alfven eigenmode in the ST40 spherical tokamak (ST) is found to be resonantly excited by thermal ions from global gyrokinetic GTC simulations. The analyses of phase-space resonances and wave-particle energy exchanges show that the Beta-induced Alfvén-Acoustic Eigenmode (BAAE) is primarily driven unstable by thermal ions, but is stabilized by energetic particles (EPs). When all kinetic effects are artificially suppressed, GTC simulations in the ideal magnetohydrodynamic (MHD) limit confirm the existence of the MHD eigenmode with a frequency in the BAAEs gap, as previously found by the ideal MHD code NOVA. The kinetic effects of thermal ions induce a frequency downshift compared to the stable BAAE in the MHD simulations. These results support the verification for global gyrokinetic simulations of the BAAE in the ST. However, the simulations do not explain the experimental observations of the BAAE in the ST40, possibly owing to the limitation of the collisionless gyrokinetic Monte Carlo model for the EPs.

Keywords: magnetic confinement fusion, spherical tokamak, Alfvén eigenmode, gyrokinetic simulation, low frequency mode

(Some figures may appear in colour only in the online journal)

* Author to whom any correspondence should be addressed.

1. Introduction

To achieve high performance in magnetic confinement fusion devices, neutral beam injection (NBI) has been extensively utilized in experiments for auxiliary heating [1]. This method could introduce massive energetic particles (EPs) into the confinement system, significantly enhancing plasma temperature and density which are critical conditions for sustained fusion reactions. However, the injection of EPs also introduces various challenges, as these particles can drive instabilities such as Alfvén eigenmodes (AEs), which affect their transport and confinement [2–4]. AEs are electromagnetic modes with discrete frequencies occurring in magnetized plasmas, which reside in the frequency gaps of the Alfvén continuum due to magnetic nonuniformity. Variations in the magnetic geometry and equilibrium profiles could influence the location and width of these frequency gaps, giving rise to multiple AEs with distinct characteristics [5, 6].

Compared with conventional tokamaks, spherical tokamaks (STs) have a much smaller aspect ratio [7], which offers several advantages, including higher plasma pressure and improved stability. On the other hand, the lower Alfvén speed in the STs leads to lower beam energy thresholds for resonant interactions between AEs and EPs and more prominent nonlinear behaviors such as rapid frequency chirping, which are more common than the conventional tokamaks [8–10]. For example, an eigenmode with frequency below toroidal AE (TAE) frequency in the ST40 has recently been observed with chirping characteristics accompanied by quasi-periodic H–L–H transitions [11–13], which can possibly have effects on quasi-periodic evolution of turbulence and transport. The ideal magnetohydrodynamic (MHD) code NOVA has identified this low frequency mode (LFM) as Beta-induced Alfvén-Acoustic Eigenmode (BAAE) [11].

BAAE is a type of AEs located near the extrema of the Alfvén-Acoustic continuum, often responsible for low-frequency electromagnetic signals observed in many fusion devices [14, 15]. Although BAAEs are often driven by EPs, thermal ions could also excite BAAEs through resonance interactions [15]. Meanwhile, kinetic theories suggest that LFMs may also exist through other mechanisms, such as the kinetic thermal ion gap [16, 17] or beta-induced ion temperature gradient eigenmodes (BTG) [18]. The multiple possible excitation mechanisms complicate their identification and interpretation of LFMs [19]. To address these complexities and kinetic effects, global gyrokinetic simulations provide a powerful approach, capturing essential kinetic effects and interactions that are critical for understanding these modes [20, 21]. The global gyrokinetic simulation code GTC [22] has been utilized extensively to study LFMs and many other AEs phenomena in conventional and STs [23–27]. For instance, GTC simulations find that kinetic effects and non-perturbative effects of thermal plasmas are crucial for the excitation of the BAAE [28]. GTC simulations of the DIII-D tokamak reveal that a sub-TAE mode is an interchange-like electromagnetic mode driven non-resonantly by pressure gradients of thermal plasmas, rather than a conventional BAAE [29]. In the JET tokamak, sub-TAE frequency electromagnetic perturbations have been identified as BTG modes [30]. Recently, GTC has been applied to investigate TAEs driven by NBI in the Mega-Amp ST (MAST) to identify the non-perturbative and kinetic effects of thermal plasmas [31].

In this work, we employ GTC to analyze the LFM observed in an ST40 experiment. We first identify the eigenmode in the fluid limit, where its mode structure is found to be similar to that obtained by ideal MHD NOVA simulations [11]. We then perform more realistic gyrokinetic simulations and analyze particle phase space structure and energy exchange between the LFM and particles. Based on its spectral position and excitation mechanism, we identify this LFM as the BAAE primarily driven unstable by thermal plasmas. These results provide a verification of global gyrokinetic simulations for studying BAAE in STs. However, our gyrokinetic simulations including the EPs find the BAAE is stabilized by it, which cannot explain the experimental observation of this LFM in the ST40.

The organization of this paper is as follows: GTC formulations are introduced in section 2. A brief description of the ST40 and the simulated shot characteristics are presented in section 3. Section 4 describes the verification of GTC simulation in the MHD limit and comparison with NOVA results. In section 5, GTC global gyrokinetic simulations of the BAAE excitation are presented. Finally, conclusions are drawn in section 6.

2. GTC gyrokinetic formulation and reduction to ideal MHD

The GTC is a particle-in-cell (PIC) code designed to simulate plasma kinetic dynamics using nonlinear gyrokinetic equations for all species including thermal ions, electrons, and EPs.

For low-frequency AE simulations, the electron drift kinetic equation is often simplified using the fluid-kinetic electron model, where its lowest-order adiabatic response is reduced to a massless fluid. By further neglecting ion kinetic effects, the gyrokinetic model can be reduced to fluid models: the two-fluid model (with finite parallel electric fields) or the ideal MHD model (without parallel electric fields). These reductions enable comparisons with MHD codes, such as NOVA [12].

In the gyrokinetic model, the evolution of the distribution function $f_s\left(R,\mu,v_{\|}\right)$ in the five-dimensional gyrocenter phase space is governed by the gyrokinetic Vlasov equation [32]

$$\left(\frac{\partial}{\partial t}+\dot{\boldsymbol{R}}\cdot\nabla+\dot{\boldsymbol{v}}_{\|}\frac{\partial}{\partial \boldsymbol{v}_{\|}}\right)f_s\left(R,\mu,v_{\|}\right)=0, \tag{1}$$

where $\mathbf{R}$ represents the gyrocenter position, $v_{\|}$ is the parallel velocity along the magnetic field line, and μ is the magnetic moment. GTC employs a perturbative (δf) simulation model, where the distribution function f_s is decomposed into an equilibrium part f_{0s} and a perturbed part δf_s.

The evolution of fields is determined by solving the gyrokinetic Poisson's equation and Ampere's law. Using the fluid-kinetic electron model [33] to avoid the numerical difficulty associated with the cancellation between parallel electrostatic and inductive electric fields, the total parallel electric

field is calculated directly from

$$\delta E_{\parallel} = -\,\mathbf{b_0}\cdot\nabla\phi_{eff}, \tag{2}$$

where $\mathbf{b_0}=\mathbf{B_0}/B_0$ is the unit vector along the magnetic field, and $\phi_{\rm eff}=\frac{T_e}{e}\frac{\delta n_e}{n_e}$ is the effective electrostatic potential calculated from electron parallel force balance using perturbed electron density, which is calculated from the electron continuity equation. As $\delta\phi$ is the electrostatic potential calculated from the gyrokinetic Poisson equation, the inductive potential is defined as $\phi_{\rm ind}=\phi_{\rm eff}-\delta\phi$. The parallel vector potential [34] $\delta A_{\parallel}$ evolves according to

$$\partial_t\delta A_{\parallel}=\mathbf{b_0}\cdot\nabla\phi_{\rm ind}. \tag{3}$$

In the current simulations, the electromagnetic fields are governed by the coupled system of the gyrokinetic Poisson equation and the perpendicular Ampere's law [35]. First, the gyrokinetic Poisson equation reduces to the quasi-neutrality condition, where the total guiding center charge density is balanced by the polarization charge density arising from ion finite Larmor radius (FLR) effects:

$$\sum_s Z_s\delta n_{{\rm pol},s}+\sum_s\delta n_s=0, \tag{4}$$

where δn_s is the perturbed guiding center density for species s, and $\delta n_{{\rm pol},s}$ represents the polarization density for species s. Second, the compressible magnetic perturbation $\delta B_{\parallel}$, which may significantly affect the low frequency Alfvénic modes [23, 24, 29], is determined by the perpendicular Ampere's law

$$\nabla\delta B_{\parallel}\times\mathbf{b_0}=\mu_0\sum_s Z_s\delta\mathbf{u}_{\perp{\rm pol},s}, \tag{5}$$

where $\delta B_{\parallel}$ is the perturbed magnetic field component parallel to the equilibrium magnetic field direction $\mathbf{B_0}$, and $\delta\mathbf{u}_{\perp{\rm pol},s}$ is the perturbed perpendicular polarization fluid velocity for species s. By assuming the scale condition $k_\perp\rho_e\ll1$ and $1/k_\perp L_p\ll1$, the two equations can be decoupled in the low-β limit, and the $\delta B_{\parallel}$ equation can be further simplified via an expansion in terms of $k_\perp\rho_s$ when $k_\perp\rho_s\ll1$ [35], where ρ_s is the gyro radius for species s and L_p is the plasma equilibrium scale length.

By neglecting ion kinetic effects, the thermal ion gyrokinetic equation can be reduced to the ion fluid equation in the long wavelength limit. To avoid the need for solving ion pressure equation, thermal ion temperature is set to be zero. The total pressure in this fluid model is entirely assigned to electrons to include the ion pressure gradient drive effect. Note that the normal GTC gyrokinetic simulation uses actual thermal ion temperature profile, which also includes the physics of ion Landau damping and all other kinetic effects. The ion continuity equation and ion parallel momentum equation in the cold ion limit read

$$\tfrac{\partial\delta n_i}{\partial t}+\nabla\cdot\left[\left(n_{0i}+\delta n_i\right)\mathbf{v_E}+n_{0i}\delta u_{\parallel i}\tfrac{\mathbf{B_0}+\boldsymbol{\delta}\mathbf{B}_\perp}{B_0}\right]=0, \tag{6}$$

$$n_{0i}\tfrac{\partial\delta u_{\parallel i}}{\partial t}+\nabla\cdot\left(n_{0i}\delta u_{\parallel i}\mathbf{v_E}\right)+\tfrac{Z_i}{m_i}n_{0i}\mathbf{b_0}\cdot\nabla\phi_{\rm eff}=0, \tag{7}$$

where $\mathbf{v_E}$ is the $E\times B$ drift velocity, $\delta u_{\parallel i}$ is the perturbed parallel ion fluid velocity, n_{0i} is the equilibrium ion density, δn_i is the perturbed ion density, and $\boldsymbol{\delta}\mathbf{B}_\perp$ is the perturbed magnetic field along perpendicular direction. The frame is also transformed to eliminate ion contributions to the parallel current, assuming $u_{\parallel 0i}=0$, while electron flow satisfies $u_{\parallel 0e}=-J_{\parallel 0}/\left(en_{0e}\right)$. This simplified two-fluid model enables extraction of radiative damping physics besides the continuum damping already contained in the ideal MHD model. The inclusion of a parallel electric field $\delta E_{\parallel}$ in the two-fluid model introduces particle acceleration, which in turn generates additional radiative damping of Alfven waves through mode conversion to kinetic Alfvén waves.

Further simplifications lead to a single-fluid ideal MHD model by enforcing $\delta E_{\parallel}=0$ and $\phi_{\rm eff}=0$. In this ideal MHD model, the ion and electron continuity equations combine into a single-fluid continuity equation

$$\begin{aligned}&\frac{\partial\delta n}{\partial t}+\mathbf{B_0}\cdot\nabla\frac{n_0\delta u_{\parallel}}{B_0}-n_0\mathbf{v}_*\cdot\frac{\nabla B_0}{B_0}+\boldsymbol{\delta}\mathbf{B}_\perp\cdot\nabla\frac{n_0\delta u_{\parallel 0}}{B_0}\\&-\frac{\nabla\times\mathbf{B_0}}{eB_0^2}\cdot\left(\nabla\delta P_{\parallel}+\frac{\left(\delta P_\perp-\delta P_{\parallel}\right)\nabla B_0}{B_0}\right)\\&+\nabla\cdot\frac{\delta P_{\parallel}b_0\nabla\times\mathbf{b_0}\cdot\mathbf{b_0}}{eB_0}+\boldsymbol{\delta}\mathbf{B}_\perp\cdot\nabla\frac{n_0\delta u_{\parallel}}{B_0}\\&-\frac{\mathbf{b_0}\times\nabla\delta B_{\parallel}}{e}\cdot\nabla\frac{\delta P_\perp+P_{\perp 0}}{B_0^2}\\&-\frac{\nabla\times\mathbf{b_0}\cdot\nabla\delta B_{\parallel}}{eB_0^2}\left(\delta P_\perp+P_{\perp 0}\right)=0,\end{aligned} \tag{8}$$

where $\delta n=\delta n_e-Z_i\delta n_i$ is the guiding center charge density, Z_i is the effective charge of the species, $\delta u_{\parallel}$ is perturbed electron parallel fluid velocity solved from parallel Ampere's Law, and $P_{\parallel}$ and $P_\perp$ stands for the pressure in parallel and perpendicular direction, respectively. Note that the guiding center charge is balanced by the ion polarization charge to enforce the quasi-neutrality condition. The field variables $\delta A_{\parallel}$ and $\delta\phi$ are solved from inductive potential $\phi_{\rm ind}=-\phi$ in the single-fluid model. Mathematically, this single-fluid model is equivalent to the ideal MHD model (e.g. as implemented in NOVA), but is based on the reduction of gyrokinetic equation in the guiding center coordinates [35, 36], which verifies that gyrokinetic equation in the fluid limit is equivalent to the ideal MHD model.

Based on these formulations, GTC could analyze various toroidal geometries and experimental settings using physics models ranging from gyrokinetic PIC simulation to two-fluid and ideal MHD models. This flexibility allows GTC to study multiple physical processes using a hierarchy of simulation models for cross-verification and isolation of each physical process.

3. Simulated ST40 experiment

As its name implies, the ST40 device has a major radius $R_0\sim$ 0.4 m and a minor radius a ~0.2 m, resulting in a relatively small aspect ratio ($A=R_0/a\sim2$) compared with conventional

tokamaks [11–13, 37]. Among ST devices, ST40 achieves notable performance enhancements with an on-axis toroidal magnetic field of around 2 T and a plasma current of about 0.6 MA, which enhances its operation. Additionally, ST40 is equipped with two tangentially injected neutral beams in the co-current direction, providing around 0.9 MW at 55 kV and 0.7 MW at 24 kV when operated with deuterium.

The ST40 discharge #09894 was selected for analysis because of its distinct transition from a steady phase to pronounced chirping behavior. During this discharge, full kinetic profile measurements were unavailable. Temperatures were instead measured using line ratios from a helium-like argon x-ray crystal spectrometer (XRCS) and a charge exchange diagnostic targeting C6+ at three radial positions on the low field side, ranging from the plasma center to mid-radius [12]. Line-integrated electron density was determined using interferometry. Plasma profiles were subsequently inferred using an integrated analysis workflow, with the TRANSP transport code applied to derive the ion temperature profile and EP density profile. These profiles are subject to an estimated 20% uncertainty [37].

Figure 1 shows the magnetic spectrogram for discharge #09894, recorded with a Mirnov coil. The spectrogram reveals the amplitude and frequency patterns of the observed chirping modes. A electromagnetic mode with a toroidal mode number $n = 1$ and poloidal harmonic number $m = 1$ was detected within the sub-TAE frequency range. This mode begins to exhibit strong frequency chirping behavior around $t = 0.092$ s, particularly in the plasma's core region. The dominant frequency lies in the range of 100–150 kHz, while the rotation frequency, inferred from charge exchange measurements, ranged from 61 to 72 kHz during this time [12]. Therefore, its mode frequency in the plasma frame could range from 38 kHz to 89 kHz.

The limited internal measurements leave open the possibility of other mode types being excited, highlighting the need for theoretical investigations. The ideal MHD code NOVA identified this mode as a BAAE [13]. Accordingly, our simulations begin with an ideal MHD analysis to verify NOVA results, followed by an extension into the gyrokinetic simulations for a more realistic examination of the mode's properties.

Figure 2 illustrates the measured density, temperature and q profiles from TRANSP run 09894A03 at $t = 0.092$ s for this shot. The on-axis parameters for this case include electron density $n_{ea} = 7.37\times10^{19}$ m^{-3}, electron temperature $T_{ea} = 4.18$ KeV, magnetic field $B_a = 1.72$ T, major radius $R_0 = 0.5$ m. Notably, ST40 features relatively strong EP density and pressure in this shot, with EPs density $n_f \sim 0.3\ n_e$ and EPs temperature $T_f \sim 3\ T_i$. Within the mode position range, the safety factor q value is approximately 1 and rapidly increases to around 14 near the edge.

4. Existence of low frequency MHD eigenmode in ST40

Our simulation begins with a linear ideal MHD model to first identify this eigenmode. For these simulations in the plasma frame, we employed a grid with $100 \times 500 \times 24$ in radial, poloidal and toroidal directions, respectively. Based on this profile and the core-localized nature of the mode, the simulation region was restricted to $\sqrt{\psi_p/\psi_p(a)} < 0.9$, encompassing the axis, where $\psi_{\rm p}$ is the poloidal magnetic flux and $\psi_{\rm p,wall}$ is the poloidal magnetic flux at the wall. Figure 2 also illustrates the profiles and boundary used in simulations, and the discrepancy in ion density arises due to the Z-effect, which characterizes the impurity content and the resulting dilution of the main ion density. In GTC, the ion density n_i is calculated using the neutrality condition, $(n_e - n_f)/Z_i$. Since GTC employs a spatially uniform effective charge Z_i while the experimental impurity profile varies radially, this approximation leads to the slight deviation between the simulated and experimental ion density profiles. To suppress numerical noise, a filter was applied to retain modes with toroidal wave number $n = 1$ and poloidal wave number $m \in [0,5]$ corresponding to the experimental observation.

Before conducting the GTC simulation, we used ALCON [38], an Alfvén continuum solver within the GTC workflow, to calculate the Alfvén-Acoustic continuum, which could provide insight into the spatial and spectral positions of the modes of interest ahead. ALCON's formulation is based on a poloidal spectral method of solving the ideal MHD Alfvén continuum equation [39], in which the coupling between Alfvenic and acoustic waves is mediated by the geodesic curvature coupling term $\kappa_s = 2\kappa \cdot B_0 \times \nabla\psi/B_0^2$. BAAE is induced by the coupling between Alfvenic and acoustic waves, therefore it is expected to lie in the so-called BAAE gap. The left panel of figure 3 shows the continuum generated by ALCON, where the thick lines represent the Alfvenic branches and thin lines represent the acoustic branches. The BAAE gap is highlighted in the low-frequency range in this figure, where the simulated frequency lies. This indicates that this low frequency eigenmode results from the coupling between Alfvén and acoustic waves. The identified eigenmode's location and frequency from the GTC antenna scan in MHD and gyrokinetic simulations are also marked and will be discussed later. For comparison, the right panel of figure 3 shows the continuum structure computed by NOVA, where the eigenmode structure is indicated by a green dashed line. In this comparison, a discrepancy is observed in the continuum structures calculated by the two codes, particularly in the core region. This discrepancy between GTC and NOVA may arise from differences in the equilibrium reconstruction, while NOVA used q solver [40] and GTC used another code called XMAP [34] to solve the Grad-Shafranov equation. However, both equilibria remain self-consistent within their respective formulations. The difference between the GTC and NOVA continua is observed to be much smaller in the region away from the magnetic axis, confirming that the deviation is localized to the reconstruction sensitivity at the core. The differences between these two equilibria are much smaller than the experimental uncertainties, and thus are not expected to change qualitatively the simulated modes.

Regarding the observed eigenmode frequency, the GTC simulation yields a frequency of 122 kHz, which differs from the 68.8 kHz calculated by NOVA. This discrepancy

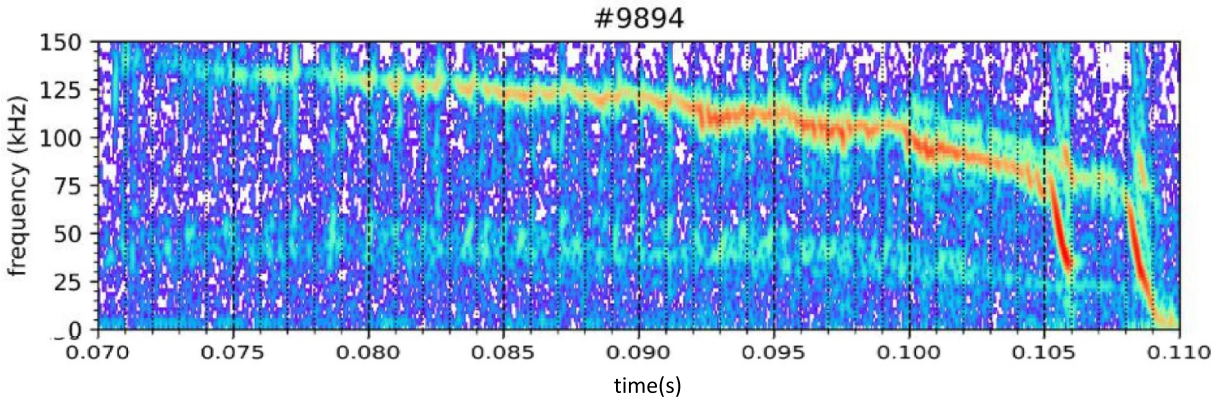

Figure 1. Spectrogram for ST40 discharge #09894. The transition from fixed frequency to chirping happens at around 0.092 s. Reproduced from [12]. © 2023 The Author(s). Published on behalf of IAEA by IOP Publishing Ltd. CC BY 4.0.

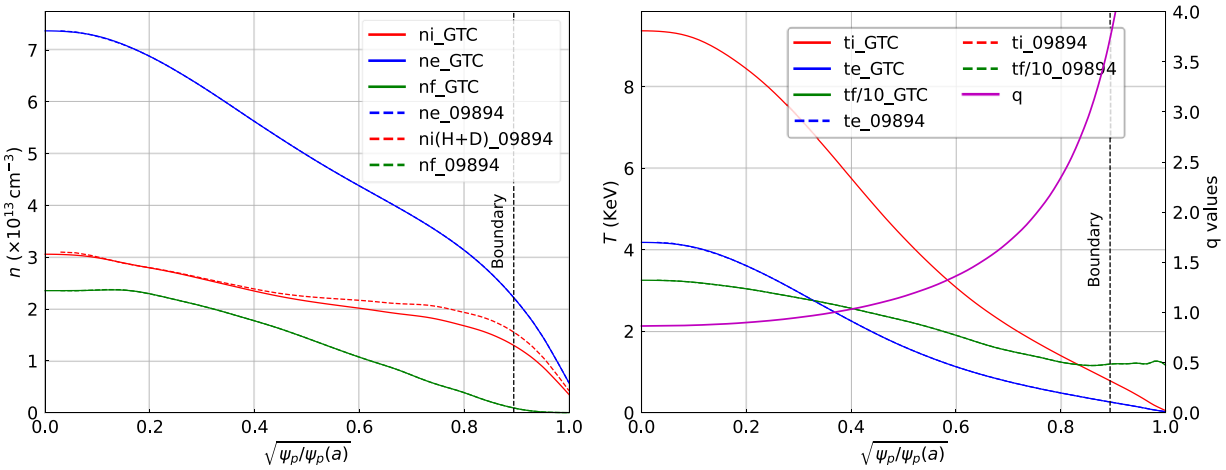

Figure 2. The density n, temperature T and safety factor q profiles of shot #09894. Solid lines show the data used in GTC simulations, while dashed lines represent the original data from TRANSP. The simulation boundary is labeled as well.

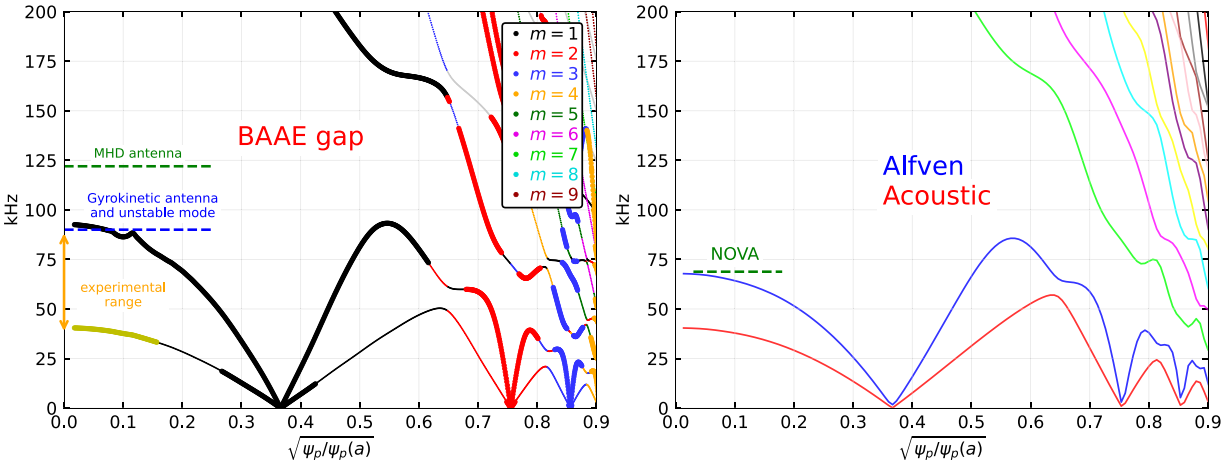

Figure 3. Left: The ALCON continua of ST40 #09894, which shows the Alfvén-acoustic continua in the sub-TAE frequency range. The BAAE gap, experimental frequency range and the eigenmode identified from GTC MHD antenna scan, gyrokinetic antenna scan and gyrokinetic unstable mode are labeled. Right: NOVA's continua from the data of [12]. The green dashed line segment shows the characteristic radial mode width. Both panels correspond to the toroidal mode number n =1. Reproduced from [12]. © 2023 The Author(s). Published on behalf of IAEA by IOP Publishing Ltd. CC BY 4.0.

first comes from their continuum difference. Using the continuum equation under the near-axis approximation with GTC parameters [14], we analytically determined the on-axis continuum frequency to be 90 kHz which is consistent with the left panel of figure 3. Although GTC, as an initial value simulation model, and the eigenmode code NOVA yield different frequency values, they both qualitatively maintain consistency by placing their respective modes within the associated spectral gap. In this comparison, the position of the identified eigenmode and the frequency contour of the continuum are similar, but their frequency exhibit some differences.

Our ideal MHD simulations start with an initial perturbation test. By introducing an initial perturbation, the numerical results show a response in the sub-TAE region with $n = 1$ and $m = 1$ perturbation, indicating the potential existence of an eigenmode. To confirm the existence of the eigenmode, we utilized the GTC antenna function to excite waves at the desired frequency, spatial location, toroidal and poloidal wave numbers. The antenna function of GTC can introduce an additional periodic signal in the form of into the system as the synthetic potential $\phi_{\rm ant}$ or parallel vector potential $\delta A_{\parallel,\rm ant}$ to drive the plasma response,

$$Y_{\rm ant} = Y_{\rm ant,0}\left(\psi\right)\cos\left(m_{\rm ant}\theta - n_{\rm ant}\zeta\right)\cos\left(\omega_{\rm ant}t\right).$$

For an existing eigenmode with frequency ω and damping rate γ, if the plasma is excited using an antenna signal with antenna frequency $\omega_{\rm ant}$ and fixed amplitude, the distribution of saturated amplitude of the induced mode will follow the formula [41]

$$A^2 \propto \frac{1}{\left(\omega^2+\gamma^2-\omega_{\rm ant}^2\right)^2+4\gamma^2\omega_{\rm ant}^2}.$$

This relationship allows us to identify the frequency ω and damping rate γ of the eigenmode by fitting the plasma's response for various antenna frequencies $\omega_{\rm ant}$. The left side of figure 4 shows the fitting result of the normalized saturated amplitudes through the antenna scan, which clearly shows the existence of an eigenmode with frequency 122 kHz and damping rate 7.08 $\times 10^4$ s^{-1}. Although the identified frequency falls outside the range of the measured result after applying the Doppler correction, it lies within the gaps generated by ALCON, as shown in figure 3. Considering the uncertainty in rotation measurement, the identified frequency from antenna scan is reasonable.

To identify the eigenmode more accurately, we can use the antenna function to induce an eigenmode near the identified frequency and then turn off the antenna. If there exists an eigenmode, the mode will naturally shift to the eigenmode frequency and decay exponentially with its damping rate γ. By analyzing this decay, we obtain a more accurate frequency f and damping rate γ. The spontaneous damping behavior is illustrated in the right side of figure 4, which provides a frequency $f = 122$ kHz and damping rate $\gamma = 2.6\times10^4$ s^{-1}.

During the decay process, the mode structure is measured and presented in the left panel of figure 5, illustrating the agreement between GTC and NOVA results in the right panel. These results confirm the existence of this eigenmode as BAAE in the ideal MHD limit, with a self-consistent frequency, damping rate, and mode structure. Furthermore, the agreement of the mode structure between GTC and NOVA serves as verification for both simulations.

5. Resonant excitation of BAAE in ST40 by thermal ions

Building on the verification of the MHD simulations, we extended the GTC simulation of ST40 discharge #09894 to include gyrokinetic ions. The electrons are described by the fluid model, and EPs are simulated using the gyrokinetic model with an equivalent Maxwellian distribution. Considering the localized radial structure of the BAAE observed in the MHD simulations, the gyrokinetic simulation boundary is reset to $\sqrt{\psi_p/\psi_p\left(a\right)} < 0.63$ to avoid a numerical instability near the outer edge. Other equilibrium and grid settings remained the same as the MHD simulations with 200 particles per cell for ions.

Without EPs, the ion density profile calculated from the charge-neutrality condition would be more inconsistent with experimental data. To address this discrepancy, the ion density gradient profile ($\kappa_{ni} = \nabla n_i/n_i$) is adjusted to match the original experimental measurement (the dotted red line in the left panel of figure 2). Under these conditions, a core localized mode of the expected range is unstable in the simulations using gyrokinetic thermal ions. Compared to the mode structure in the MHD simulation shown in figure 5, the gyrokinetic mode structure in figure 6(*a*) lacks a radial zero-crossing point near the magnetic axis, which may be due to the large ion banana orbit effects near the axis. In contrast, the MHD simulations typically exhibit more distinct singularity properties of the mode structures. The unstable BAAE has a real frequency $f = 90$ kHz and a growth rate γ corresponding to $\gamma/\omega_r \sim 0.06$. Under the simulation parameters, the ion diamagnetic drift frequency for this case was approximately 100 kHz. Setting the ion density gradient $\kappa_{ni} = 0$ but keeping temperature gradient could stabilize the mode. An antenna scan in gyrokinetic simulations is also conducted under this stable condition without ion density gradient, which shows an eigenfrequency of approximately 90 kHz. This frequency differs from the 122 kHz frequency identified in GTC ideal MHD simulations, but very close to the unstable BAAE frequency in the gyrokinetic simulation with actual thermal ion density gradient. The discrepancy suggests that kinetic effects are responsible for the observed frequency downshift from the GTC ideal MHD simulations without ion density gradient effects. The thermal ion kinetic effects contribute as second-order terms to the MHD equations. In our simulations, we observe that these kinetic terms modify the growth rate (the imaginary part of the eigenfrequency) by a magnitude of order ~0.1. Consequently, it is physically consistent that these kinetic contributions also introduce a correction of a similar order to the real part of the frequency, resulting in the observed downshift. These results

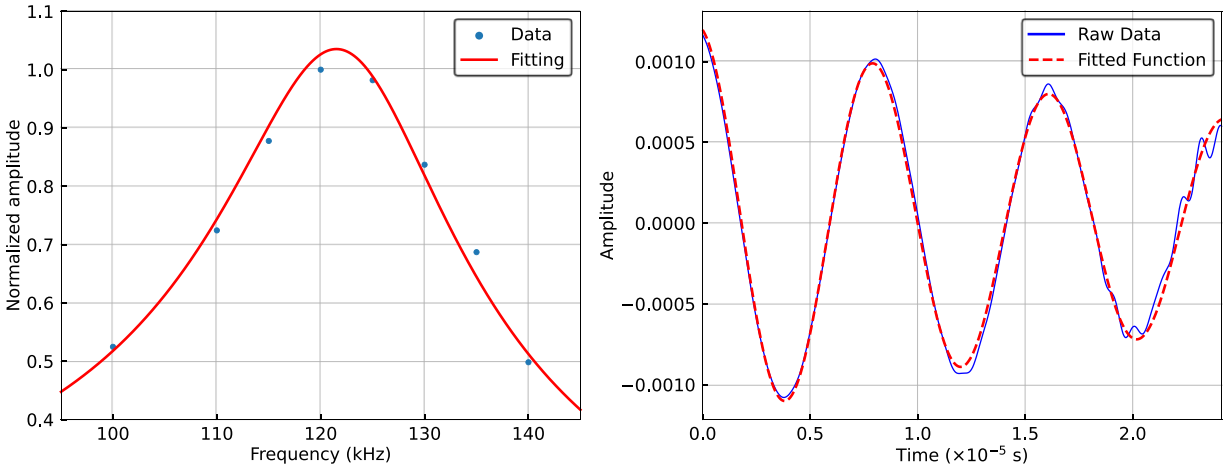

Figure 4. Left: Antenna frequency scan in GTC ideal MHD simulations shows a low frequency eigenmode. The x-axis represents the frequency, while the y-axis represents the normalized response amplitude. Right: Decay of eigenmode after 125 kHz antenna excitation.

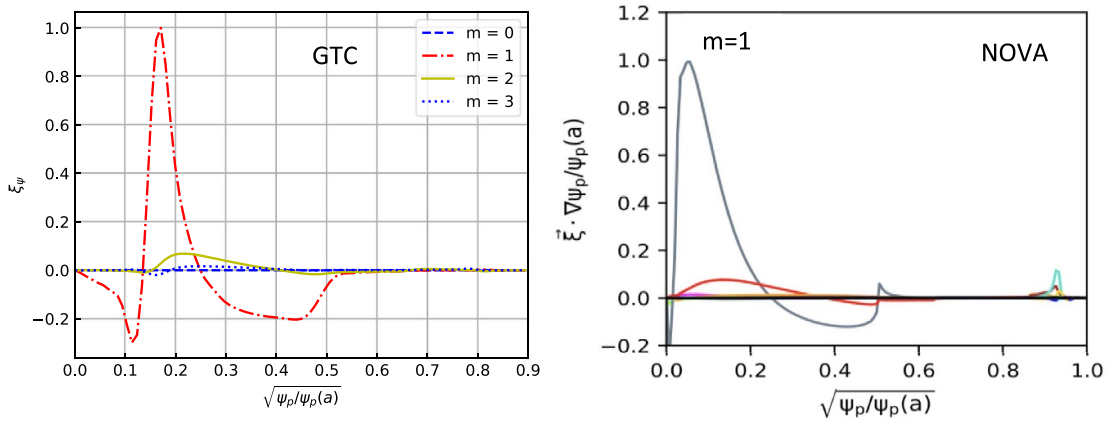

Figure 5. Radial damped mode structure in GTC compared with NOVA. The left panel is GTC's mode structure measured at 5 $\times 10^{-6}$ s in figure 4 (right), and the right panel is generated by NOVA taken from [12], the vertical axes in both panels represent the same quantity. Reproduced from [12]. © 2023 The Author(s). Published on behalf of IAEA by IOP Publishing Ltd. CC BY 4.0.

confirm that the modes observed in gyrokinetic and MHD simulations are the same branch and that the kinetic effects of the thermal ions play an important role in the BAAE excitation.

We then included the EPs in the GTC gyrokinetic simulations using local Maxwellian distribution function. The EPs are treated using the collisionless gyrokinetic Monte-Carlo model. In this approach, the fast ions are represented by marker particles that follow the gyrokinetic equations of motion. This formulation retains kinetic effects, such as FLR and wave-particle resonances, which are critical for studying the interaction between EPs and AEs. As the EP density gradually increased from 0 to its actual value, the BAAE instability was weakened and eventually damped entirely. Extending the distribution of EPs to Slowing-down distribution still fails to enable us to observe the LFM. These findings suggest that the observed BAAE is primarily driven by thermal plasmas rather than EPs. The possibility for such excitation was pointed out in the earlier publication due to the temperature gradient drive of thermal ions [15]. The current GTC results, however, present a significant discrepancy with experimental observations, which show the presence of this mode even under conditions where a non-negligible EPs population exists. Possible explanations for this discrepancy may include the effects of realistic EPs distribution function and the uncertainties of profile measurements, especially thermal and EPs densities and temperatures. Specifically, an isotropic Maxwellian distribution was used to represent the EPs. However, NBI in ST40 generates a highly anisotropic slowing-down distribution. By assuming isotropy, the simulation model may artificially populate phase-space regions that induce strong continuum or resonance damping—regions that might be devoid of particles in the actual anisotropic distribution—thereby overestimating the stabilizing effect. Additionally, the strong frequency chirping observed in the experiment indicates significant nonlinear physics which could not been modeled by current linear simulation. While the qualitative behavior of the mode's response to fast particles is instructive, a quantitative reconciliation between our simulation results and the experimental data will

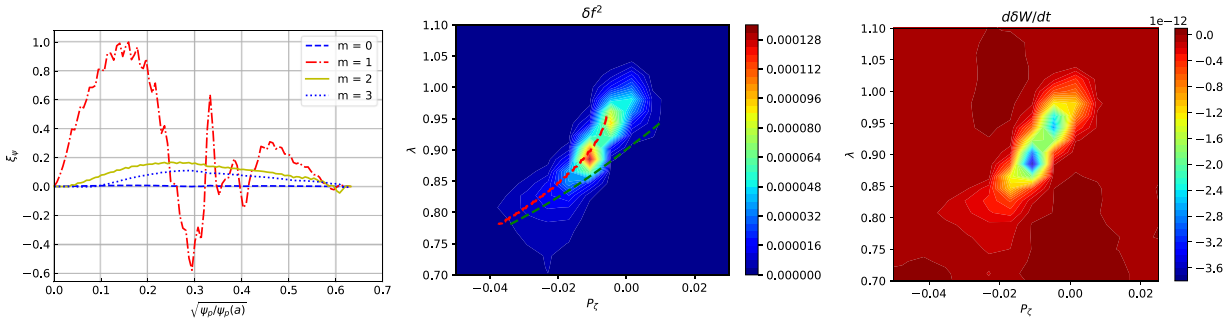

Figure 6. (a) Radial mode structure in GTC gyrokinetic simulation. (b) The δf^2 distribution in (P_ζ, λ) space for particles with μ value ranging from 1.1 E_0/B_a to 1.85 E_0/B_a. The red dashed line is the boundary between passing particles and trapped particles, while the green dashed line is where the transit frequency of ion coincides with the low frequency wave. (c) Wave-particle energy exchange rate of ions distribution in (P_ζ, λ) space for particles with μ value ranging from 1.1 E_0/B_a to 1.85 E_0/B_a.

require future nonlinear simulations utilizing realistic, anisotropic distribution functions, and is beyond the scope of this study and represents a critical area for future investigation.

To investigate the drive mechanism of this BAAE, we examined the resonances of the thermal ions by analyzing the phase-space structures in our simulation. The δf^2 of the thermal ions as a function of the magnetic moment μ exhibits a peak around $\mu B_a = 1.5E_0$, where E_0 is the on-axis ion temperature $T_{ion,\,a}$. This indicates that the resonances are strongest for particles at $\mu = 1.5\ E_0/B_a$. To further analyze these resonances, we selected those ions with the μ value ranging from 1.1 E_0/B_a to 1.85 E_0/B_a and plotted their δf^2 distribution in (P_ζ, λ) space. Here, $\lambda = \mu B_a/E$ represents the pitch angle and $P_\zeta = gv_\parallel/B - \psi_{\rm p}$ is the canonical angular momenta, where $\psi_{\rm p}$ is the poloidal magnetic flux and g represents poloidal current and appears in the covariant representation of magnetic field $B = g\nabla\zeta + I\nabla\theta + \delta\nabla\psi$ using Boozer coordinates.

Figure 6(b) illustrates the δf^2 distribution in phase space (P_ζ, λ). Since the magnetic moment μ has a small range the variation in λ primarily represents changes in the particle energy E. The red dashed line in figure 6(b) marks the boundary between passing particles and trapped particles, while the green line is where the transit frequency of ions coincides with the BAAE frequency. The overlap of the δf^2 response with the trapped-passing boundary and the transit frequency of the passing particles shows location in the phase space for the resonances between thermal ions and the waves occur.

Furthermore, GTC has the capability to measure the rate of wave-particle energy exchange, providing insights into the energy transfer between particles and waves. The energy change of the particles is calculated using the formula

$$\frac{d\delta W}{dt} = \left\langle -Ze\left(v_\parallel \frac{B^*}{B^*_\parallel} + \frac{\mu}{Z}\,\mathbf{b_0}\times\frac{\nabla B_0}{B^*_\parallel}\right)\cdot\nabla\phi - Z_s e v_\parallel \frac{\partial \delta A_\parallel}{\partial t}\right\rangle,$$

where $Z_s e$ is the particle charge, $B^* = B^*_0 + \delta B_\perp = B_0 + \frac{m_s v_\parallel}{Z_s}\nabla\times b_0 + \delta B_\perp$, $v_\parallel$ is the guiding center parallel velocity and $\partial\delta A_\parallel/\partial t$ is calculated through $\partial_t \delta A_\parallel = \mathbf{b_0}\cdot\nabla\phi_{\rm ind}$ as discussed in section 2. The brackets represent a flux-surface average and a gyrocenter velocity-space integral, weighted by the perturbed distribution function.

Figure 6(c) is the ions wave-particle energy exchange rate distribution in the (P_ζ, λ) space, which shows a similar pattern as figure 6(b). Such a distribution confirms the resonance between ions and the LFM. Besides, using this formula, the wave-particle energy exchange rate can be separated into contributions from the perpendicular and parallel directions. Figure 7(a) presents the normalized radial wave-energy exchange rate for ions. These results also indicate that energy transfer occurs from particles to the wave, i.e. $\frac{{\rm d}\delta W}{{\rm d}t} < 0$, with most of the energy exchange happening in the perpendicular direction, and their radial distribution aligns with the mode location.

The wave polarization can be further studied to understand features of the mode of interest. The diagnosis of the parallel electric field $E_\parallel$ and its electrostatic component $E_{\parallel,es}$ can be utilized to infer whether the induced mode is Alfvénic or acoustic, because ideal Alfvén waves have $E_\parallel/E_{\parallel,es} = 0$ while electrostatic waves have $E_\parallel/E_{\parallel,es} = 1$. The induced BAAE is characterized by a strong acoustic polarization, as $E_\parallel/E_{\parallel,es}$ reaches 0.5 near the axis. Besides, GTC can simulate scenarios both with and without the parallel perturbed magnetic field $\delta B_\parallel$, which has been shown to play a crucial role in low-frequency electromagnetic simulations [35]. With $\delta B_\parallel$ added, the BAAE frequency decreased slightly to 68 kHz with similar radial structures and growth rate. The structure of $\delta B_\parallel$ and $\delta B_\perp$ are depicted in figure 7(b), which shows that the $\delta B_\parallel$ is about half of the $\delta B_\perp$ in this BAAE. These properties and excitation mechanisms are similar to the LFM in the DIII-D tokamak which is an interchange-like mode driven by the pressure gradient of thermal plasmas [29]. However, while the DIII-D LFM was detectable in the simulations with EPs [29], the BAAE in this ST40 shot was not observed in the simulations with EPs.

Additional simulations with EPs were conducted by varying the thermal ion beta ($\beta_{\rm i}$) by changing ion temperature $T_{\rm i}$ while keeping the total beta constant. Interestingly, as thermal ion β_i increased from the experimental value, the growth rate and frequency of the mode remained relatively

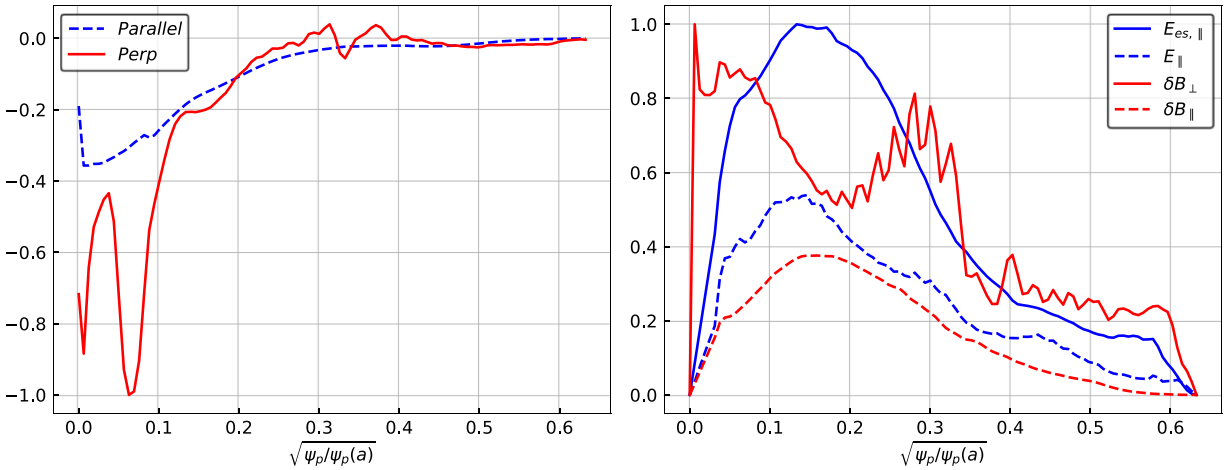

Figure 7. (*a*) The radial structure of normalized wave-particle energy exchange rate $\mathrm{d}\delta W/\mathrm{d}t$ of ions in parallel and perpendicular directions. (*b*) The radial structure of parallel electric field $E_\parallel$, its electrostatic component $E_{\parallel,es}$, as well as the parallel and perpendicular magnetic perturbations $\delta B_\parallel$ and $\delta B_\perp$, both electric and magnetic perturbations are normalized, respectively, by their maximal values.

unchanged. Conversely, when thermal ion β_i decreased from the experimental value, the low-frequency signal weakened, further supporting the hypothesis that this mode is predominantly driven by thermal ions.

Finally, a scan over toroidal mode numbers $n = 2,3,4$ did not reveal any instabilities to compare their real frequency, as the predictions of Beta-induced Temperature Gradient (BTG) theory suggests that the mode frequency should scale with the toroidal mode number n, according to the formula for the diamagnetic drift frequency ω_i^* [30].

6. Conclusion

In this study, the excitation mechanisms of a low-frequency AE in the ST40 were analyzed using the global gyrokinetic code GTC. In the GTC ideal MHD limit, simulations confirmed the existence of an MHD eigenmode within the BAAE gap, consistent with the results of the ideal MHD code NOVA and showing similar mode structures. In the GTC gyrokinetic simulations, this BAAE was driven unstable by thermal plasmas in the absence of EPs. The inclusion of kinetic effects of thermal ions induces a frequency downshift and makes the mode structure more regular in the excited BAAE in the gyrokinetic simulations compared to the stable mode in the MHD simulations. When EPs were included, the instability weakened and was eventually suppressed as their density increased. However, this contradicts experimental data where the mode persists despite a significant EP population. Phase-space resonance analysis showed that the mode resonates with thermal ions, and energy exchange indicated that thermal ions drive the mode. The observed polarization shows a strong acoustic polarization, while $\delta B_\parallel$ effects slightly reduced the mode frequency but had little effects on the growth rate.

To further investigate the driving mechanisms of this mode, simulations with more well-diagnosed experimental shots and actual EPs distribution are needed. Future studies will aim to extend the simulations to the nonlinear regime to explore the impact of this mode on turbulence and transport, as well as its potential role in the H–L–H transition [11].

Acknowledgment

We would like to thank Henry Hingyin Wong for useful discussions. This work was supported by DOE INCITE and Grant DE-SC0021316. Simulations used computing resources at ORNL (DOE Contract DE-AC05-00OR22725) and NERSC (DOE Contract DE-AC02-05CH11231).

ORCID iDs

Handi Huang 0000-0002-7645-9454
Nikolai Gorelenkov 0000-0002-7345-8149
Xishuo Wei 0000-0001-7486-0407
Zhihong Lin 0000-0003-2007-8983
V.N. Duarte 0000-0001-8096-7518
Stanley Kaye 0000-0002-2514-1163
Michele Romanelli 0000-0003-4897-4843

References

[1] Kelley G.G., Morgan O.B., Stewart L.D., Stirling W.L. and Forsen H.K. 1972 Neutral-beam-injection heating of toroidal plasmas for fusion research *Nucl. Fusion* **12** 169
[2] Fasoli A. *et al* 2007 Chapter 5: physics of energetic ions *Nucl. Fusion* **47** S264
[3] Heidbrink W.W. 2008 Basic physics of Alfvén instabilities driven by energetic particles in toroidally confined plasmas *Phys. Plasmas* **15** 055501
[4] Salewski M. *et al* 2025 Energetic particle physics: chapter 7 of the special issue: on the path to tokamak burning plasma operation *Nucl. Fusion* **65** 043002
[5] Cheng C.Z., Chen L. and Chance M.S. 1985 High-*n* ideal and resistive shear Alfvén waves in tokamaks *Ann. Phys.* **161** 21–47
[6] Chen L. and Zonca F. 2016 Physics of Alfvén waves and energetic particles in burning plasmas *Rev. Mod. Phys.* **88** 015008

[7] Kaye S.M., Connor J.W. and Roach C.M. 2021 Thermal confinement and transport in spherical tokamaks: a review *Plasma Phys. Control. Fusion* **63** 123001

[8] Crocker N.A. *et al* 2008 Alfvén cascade modes at high β in the National Spherical Torus Experiment *Phys. Plasmas* **15** 102502

[9] Fredrickson E.D. *et al* 2012 Fast-ion energy loss during TAE avalanches in the National Spherical Torus Experiment *Nucl. Fusion* **53** 013006

[10] Duarte V.N., Berk H.L., Gorelenkov N.N., Heidbrink W.W., Kramer G.J., Nazikian R., Pace D.C., Podestà M., Tobias B.J. and Van Zeeland M.A. 2017 Prediction of nonlinear evolution character of energetic-particle-driven instabilities *Nucl. Fusion* **57** 054001

[11] Bland J., Varje J., Gorelenkov N.N., Gryaznevich M.P., Sharapov S.E. and Wood J. T. T. ST40 2022 Interplay between beam-driven chirping modes and plasma confinement transitions in spherical tokamak ST40 *Nucl. Fusion* **63** 016024

[12] Duarte V.N., Gorelenkov N.N., Kaye S.M., Bonofiglo P.J., Podestà M., Bland J., Buxton P., Gryaznevich M., Romanelli M. and Sertoli M. 2023 Perturbative analysis of low-frequency instabilities in high-field ST40 experiments *Nucl. Fusion* **63** 036018

[13] McNamara S.A.M. *et al* 2024 Overview of recent results from the ST40 compact high-field spherical tokamak *Nucl. Fusion* **64** 112020

[14] Gorelenkov N.N., Berk H.L., Fredrickson E. and Sharapov S.E. (JET EFDA Contributors) 2007 Predictions and observations of low-shear beta-induced shear Alfvén–acoustic eigenmodes in toroidal plasmas *Phys. Lett. A* **370** 70

[15] Gorelenkov N.N., Van Zeeland M.A., Berk H.L., Crocker N.A., Darrow D., Fredrickson E., Fu G.-Y., Heidbrink W.W., Menard J. and Nazikian R. 2009 Beta-induced Alfvén-acoustic eigenmodes in National Spherical Torus Experiment and DIII-D driven by beam ions *Phys. Plasmas* **16** 056107

[16] Zonca F., Chen L. and Santoro R.A. 1996 Kinetic theory of low-frequency Alfvén modes in tokamaks *Plasma Phys. Control. Fusion* **38** 2011

[17] Chen L. and Zonca F. 2007 Theory of Alfvén waves and energetic particle physics in burning plasmas *Nucl. Fusion* **47** S727

[18] Mikhailovskii A.B. and Sharapov S.E. 1999 Beta-induced temperature-gradient eigenmodes in tokamaks: I. General ideas and MHD theory *Plasma Phys. Rep.* **25** 803–16 (available at: https://www.osti.gov/etdeweb/biblio/20419450)

[19] Heidbrink W.W., Van Zeeland M.A., Austin M.E., Bierwage A., Chen L., Choi G.J., Lauber P., Lin Z., McKee G.R. and Spong D.A. 2021 BAAE' instabilities observed without fast ion drive *Nucl. Fusion* **61** 016029

[20] Lee W.W. 1983 Gyrokinetic approach in particle simulation *Phys. Fluids* **26** 556

[21] Lee W.W. 1987 Gyrokinetic particle simulation model *J. Comput. Phys.* **72** 243

[22] Lin Z., Hahm T.S., Lee W.W., Tang W.M. and White R.B. 1998 Turbulent transport reduction by Zonal Flows: massively parallel simulations *Science* **281** 1835

[23] Liu P., Wei X., Lin Z., Brochard G., Choi G.J., Heidbrink W.W., Nicolau J.H. and McKee G.R. 2022 Regulation of Alfvén eigenmodes by microturbulence in fusion plasmas *Phys. Rev. Lett.* **128** 185001

[24] Brochard G. *et al* 2024 Saturation of fishbone instability by self-generated zonal flows in tokamak plasmas *Phys. Rev. Lett.* **132** 075101

[25] Wang Z., Lin Z., Holod I., Heidbrink W.W., Tobias B., Van Zeeland M. and Austin M.E. 2013 Radial localization of toroidicity-induced Alfven eigenmodes *Phys. Rev. Lett.* **111** 145003

[26] Zhang H.S., Liu Y.Q., Lin Z. and Zhang W.L. 2016 Gyrokinetic particle simulation of beta-induced Alfven-acoustic eigenmode *Phys. Plasmas* **23** 042510

[27] Cheng J., Zhang W., Lin Z., Li D., Dong C. and Cao J. 2017 Nonlinear co-existence of beta-induced Alfvén eigenmodes and beta-induced Alfvén-acoustic eigenmodes *Phys. Plasmas* **24** 092516

[28] Liu Y., Lin Z., Zhang H. and Zhang W. 2017 Excitation of low frequency Alfven eigenmodes in toroidal plasmas *Nucl. Fusion* **57** 114001

[29] Choi G.J., Liu P., Wei X.S., Nicolau J.H., Dong G., Zhang W.L., Lin Z., Heidbrink W.W. and Hahm T.S. 2021 Gyrokinetic simulation of low-frequency Alfvénic modes in DIII-D tokamak *Nucl. Fusion* **61** 066007

[30] Fil N. *et al* 2021 Interpretation of electromagnetic modes in the sub-TAE frequency range in JET plasmas with elevated monotonic q-profiles *Phys. Plasmas* **28** 102511

[31] Wong H.H. *et al* 2024 Linear gyrokinetic simulations of toroidal Alfvén eigenmodes in the Mega-Amp Spherical Tokamak *Phys. Plasmas* **31** 112508

[32] Brizard A.J. and Hahm T.S. 2007 Foundations of nonlinear gyrokinetic theory *Rev. Mod. Phys.* **79** 421

[33] Lin Z. and Chen L. 2001 A fluid–kinetic hybrid electron model for electromagnetic simulations vol 4

[34] Wei X., Choi G., Brochard G., Liu P., Lin Z. and Bao J. 2021 Electromagnetic formulations for GTC simulation (arXiv:2109.08873)

[35] Dong G., Bao J., Bhattacharjee A., Brizard A., Lin Z. and Porazik P. 2017 Gyrokinetic particle simulations of the effects of compressional magnetic perturbations on drift-Alfvenic instabilities in tokamaks *Phys. Plasmas* **24** 081205

[36] Deng W., Lin Z. and Holod I. 2012 Gyrokinetic simulation model for kinetic magnetohydrodynamic processes in magnetized plasmas *Nucl. Fusion* **52** 023005

[37] McNamara S.A.M. *et al* 2023 Achievement of ion temperatures in excess of 100 million degrees Kelvin in the compact high-field spherical tokamak ST40 *Nucl. Fusion* **63** 054002

[38] Deng W., Lin Z., Holod I., Wang Z., Xiao Y. and Zhang H. 2012 Linear properties of reversed shear Alfvén eigenmodes in the DIII-D tokamak *Nucl. Fusion* **52** 043006

[39] Cheng C.Z. and Chance M.S. 1985 Low-n shear Alfven spectra in axisymmetric toroidal plasmas *No. PPPL-2286* (Princeton Plasma Physics Lab. (PPPL))

[40] DeLucia J., Jardin S.C. and Todd A.M.M. 1980 An iterative metric method for solving the inverse tokamak equilibrium problem *J. Comput. Phys.* **37** 183

[41] Zhang H.S., Lin Z., Holod I., Wang X., Xiao Y. and Zhang W.L. 2010 Gyrokinetic particle simulation of beta-induced Alfvén eigenmode *Phys. Plasmas* **17** 112505